Journal of Alloys and Compounds 806 (2019) 668–675

Contents lists available at ScienceDirect

Journal of Alloys and Compounds

journal homepage: http://www.elsevier.com/locate/jalcom

Effect of Hf substitution Cu on glass-forming ability, mechanical properties and corrosion resistance of Ni-free Zr–Ti–Cu–Al bulk metallic glasses

Z.S. Jin [a], Y.J. Yang [a], Z.P. Zhang [a], X.Z. Ma [a, b], J.W. Lv [a], F.L. Wang [a], M.Z. Ma [a, *], X.Y. Zhang [a], R.P. Liu [a]

[a] State Key Laboratory of Metastable Materials Science and Technology, Yanshan University, Qinhuangdaom, 066004, China
[b] College of Materials Science and Engineering, Beijing University of Technology, Beijing, 100124, China

ARTICLE INFO

Article history:
Received 26 April 2019
Received in revised form
18 July 2019
Accepted 20 July 2019
Available online 20 July 2019

Keywords:
Glass-forming ability
Substitution of Hf with Cu
Zr-based bulk metallic glasses
Mechanical properties
Corrosion behavior

ABSTRACT

A series of Ni-free $Zr_{55}Ti_3Hf_xCu_{32-x}Al_{10}$ ($x = 0$, 1, 2, 3, 4, 5 at. %) bulk metallic glasses (BMGs) were developed by copper mold suction-casting. The effect of partially substituting Cu by Hf was investigated in terms of glass-forming ability (GFA), mechanical properties, and corrosion behavior. As a result of the partial substitution, the GFA of Hf-bearing amorphous alloys were significantly enhanced as compared to $Zr_{55}Ti_3Cu_{32}Al_{10}$ BMGs. Hf addition also enlarged the supercooled liquid region from 55 K to 70 K. The critical diameter was found to increase from 4 mm to 8 mm for $x = 3$. The corresponding compressive yield strength was over 1800 ± 21 MPa with a large plastic strain above 2.60 ± 0.10%. Electrochemical tests indicated that the lowest corrosion current density was $1.6 \pm 0.1 \times 10^{-8}$ A/cm^2 for the alloy with $x = 5$ in H_2SO_4 solution, thereby yielding a superior corrosion resistance.

1. Introduction

Bulk metallic glasses (BMGs) have attracted significant research interest since their superior or unique mechanical and physical properties compared to their crystalline materials, such as high strength, great elastic strain limit, relatively low Young's modulus, magnetic properties, excellent corrosion and wear resistance, etc [1–4]. BMGs exhibit excellent application potential in various field, such as consumer electronics, catalysts, medical devices, and solar energy conversion, owing to their unique structures and unusual properties [5]. Up to now, a series of amorphous systems have been developed, based on Zr- [6], Cu- [7], Mg- [8], Fe- [9], Ti-based [10] BMGs. The large critical diameter (d_c) greater than 15 mm have been found in many BMGs systems, such as Zr-Ti-Cu-Ni-Be [6] and Zr–Cu–Al–Ni–Nb [11] alloy systems. Generally, Zr-based BMGs have high GFA, great toughness and fracture strength, which are most promising structural materials [12] among these BMGs systems. It was found that the toxic elements, including Be and Ni, maintain composition with high GFA in Zr-based BMGs. When such BMGs come in direct contact with human skin or body fluids, they can release Ni, Be, which are allergens and carcinogens [13]. The existence of Ni and Be as constituent elements have seriously restricted the applications of Zr-based BMGs for biomaterials. Therefore, there is a need for Ni-free or Be-free BMGs system with high GFA and great mechanical properties. Minor additions of alloying elements into BMGs [14–16] has been an effective way to develop novel amorphous alloy. In general, these new amorphous alloys have superior GFA, great mechanical properties and corrosion resistance also were enhanced [17]. For example, addition of elements, such as Ag [18], Pd [19], has significantly improved the GFA and mechanical properties of amorphous alloys, such as Zr–Cu–Al–Ag [18], Zr-Cu-Pd-Al-Ag [20], Zr–Al–Co–Ag [21] BMGs systems. However, most of these BMGs have high content of Ag and Pd, which increases the cost of the preparation of alloys. Hence, it has been the goal of researchers in the amorphous alloys field to find low-cost alternatives to improve the GFA of amorphous alloys. Recently, the addition or substitution Hf has been reported to improve the GFA and engineering properties of BMGs [23-25]. Most reports have focused on the influence of Zr substitution by Hf, whereas the influence of partial substitution of Cu by Hf on the GFA,

* Corresponding author. State Key Laboratory of Metastable Materials Science and Technology, Yanshan University, Qinhuangdao, 066004, China.
E-mail address: mz550509@ysu.edu.cn (M.Z. Ma).

https://doi.org/10.1016/j.jallcom.2019.07.240
0925-8388/

mechanical properties and corrosion resistance of BMGs has not been fully explored. Additionally, the corrosion resistance of Zr-based BMGs with high content of Cu is inferior compared to the Cu-free amorphous in chloride-ion-containing solutions [22,23]. Hence, partial substitution of Cu by Hf could aid in the development of new BMGs with higher GFA, great mechanical properties and excellent corrosion resistance.

In this work, based on the $Zr_{55}Ti_3Cu_{32}Al_{10}$ alloy, novel $Zr_{55}Ti_3Hf_xCu_{32-x}Al_{10}$ amorphous alloys were prepared by partial substituting Cu by Hf. The influence of this partial substitution was investigated by studying the GFA, mechanical properties and corrosion behaviors.

2. Experimental procedure

Master alloy ingots with nominal atomic percentage of $Zr_{55}Ti_3Hf_xCu_{32-x}Al_{10}$ ($x = 0$, 1, 2, 3, 4 and 5 at.%) were synthesized with high purity metals by arc-melting under a high-purity argon atmosphere. The raw materials with purity higher than 99.99% were used as the alloy ingots and master ingots need to be melted five times to ensure uniformity of composition. Then, cylindrical alloy rods with different diameters of 3, 5, 6 and 8 mm were preparing by copper mold suction-casting. X-ray diffraction (XRD, D/max-2500/PC) with Cu Kα radiation and transmission electron microscopy (TEM, JEOL-2010) were used to examine the microstructure and crystalline state of the cast rods. The thermal parameters of BMGs were obtained by using differential scanning calorimeter (DSC, Nestzsch STA449C) at a heating rate of 20 K/min. An Instron 5982 testing machine was used to measure the mechanical properties of the samples with a diameter of 3 mm and a length of 6 mm at an engineering strain rate of 5×10^{-4} s^{-1}. The specimen for compression experiment were repeated at least 4 times. The morphology of alloy specimens were observed by using scanning electron microscopy (SEM, Hitachi S-3400). Conventional three-electrode cell system was carried out to the electrochemical measurements, comprising of a platinum electrode as assistant electrode, a saturated calomel electrode was used as standard electrode and the corrosion samples as the working electrode. The samples were cut into a cylindrical size of $\varphi 3 \times 4$ mm and ground with 3000 grit SiC sandpapers. The surface of the samples were polished with a diamond polishing paste. Before electrochemical measurements, the samples were cleaned in deionized water and ethanol. In order to maintain the stability of open-circuit potentials, the samples were immersed in the solutions for 30 min. The electrochemical experiments tests were carried out in 0.6 mol/L NaCl, 1 mol/L HCl, and 1 mol/LH_2SO_4 electrolytes solutions.

3. Results and discussions

3.1. Microstructures

Fig. 1 shows typical XRD patterns of as-casting $Zr_{55}Ti_3Hf_xCu_{32-x}Al_{10}$ ($x = 0$, 1, 2, 3, 4 and 5 at. %) rod alloys and the critical diameters can be achieved. The XRD patterns exhibited a broad diffraction feature near $2\theta = 38°$ without any detectable sharp Bragg crystalline peaks, which was indicative of a glassy structure. Although, the critical diameter of original alloy was 4 mm, substitution of Cu with Hf resulted in a maximum critical diameter of 8 mm for the alloy with $x = 3$, which was twice that of Hf-free $Zr_{55}Ti_3Cu_{32}Al_{10}$. Hf addition of 1–5 at. % significantly improved the GFA of the BMGs. TEM observation was done in order to further investigate the glassy structure of as-prepared alloys. Bright-field TEM images, selected area electron diffraction (SAED) patterns and high-resolution transmission electron microcopy (HRTEM) image of $Zr_{55}Ti_3Hf_xCu_{32-x}Al_{10}$ ($x = 0$ and 3) are shown in Fig. 2. From the TEM analysis there was no evidence of nano-crystalline phases, crystalline fringes or phase separation. The SAED patterns also consisted only of halo rings, indicating a purely amorphous structure of as-prepared alloys. The microstructure results of alloys are highly consistent with the observation from XRD patterns results.

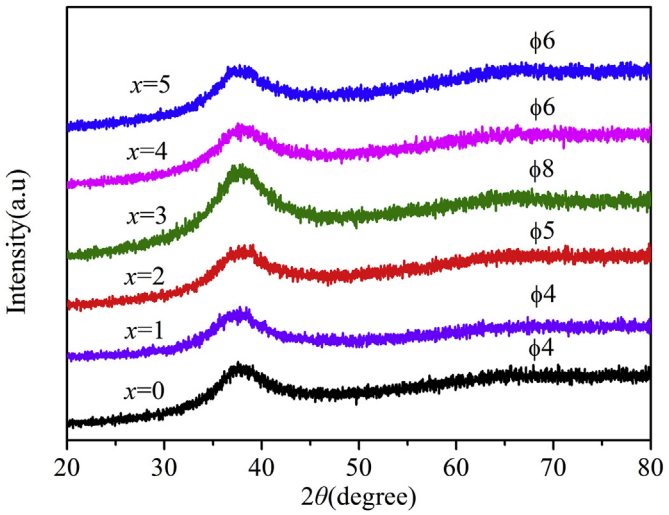

Fig. 1. XRD patterns of $Zr_{55}Ti_3Hf_xCu_{32-x}Al_{10}$ ($x = 0$, 1, 2, 3, 4 and 5 at.%) glassy rods with their critical diameters.

3.2. GFA and thermal stability

Fig. 3 shows the DSC curves of $Zr_{55}Ti_3Hf_xCu_{32-x}Al_{10}$ ($x = 0$, 1, 2, 3, 4 and 5 at. %) amorphous alloys at a heating rate of 20 K/min. From the DSC curves, it was evident that all alloys exhibited an obvious glass transition followed by a wide supercooled liquid region, and then the production of exothermic peaks corresponding with crystallization. Table 1 shows the summary of the relevant thermodynamic parameters, such as glass transition temperature (T_g), crystallization temperature (T_x), melting temperature (T_m), liquids temperature (T_l), the supercooled liquid region ($\Delta T = T_x - T_g$), reduced glass transition temperature ($T_{rg} = T_g/T_l$) and γ value ($\gamma = T_x/(T_g + T_l)$). T_g and T_x gradually increased with increasing in the content of Hf. ΔT obtained a maximum value of 70 K for $x = 2$. When the Hf content was 3 at. %, T_l also reached a minimum of 1124 K. The results showed the width of the supercooled temperature region ΔT_x was increased. This feature was indicative of the resistance to crystallization of the supercooled liquid. Moreover, when Cu was gradually substituted by Hf, the crystallization process changed from a two-stage event to a single-peak process, which was suggestive of the crystallization behavior being strongly dependent on the alloy compositions. Hf substitution changed the internal structure of BMGs and affected crystallization process. The $Zr_{55}Ti_3Hf_3Cu_{29}Al_{10}$ alloy exhibited the lowest T_l, reflecting that this amorphous alloy composition was closer to the eutectic point as compared to Hf-free BMGs. The lower T_l of the deep eutectic composition, the higher stability of molten liquid phase in the thermodynamic. Accordingly, the atomic rearrangement became difficult and destabilize the process of nucleation of crystal nucleus. As well as the growth of crystallization phases were inhibited [26], thereby promoting the glassy phase formation. Generally, BMGs with lower T_l showed good GFA [27].

Furthermore, It is known that the atomic size difference (δ), the mixing enthalpy (ΔH_{mix}), the mixing entropy(ΔS_{mix}), electronegativity difference ($\Delta\chi$) and valence electron concentration (VEC) have effect on the GFA [28,29]. The relevant values were calculated

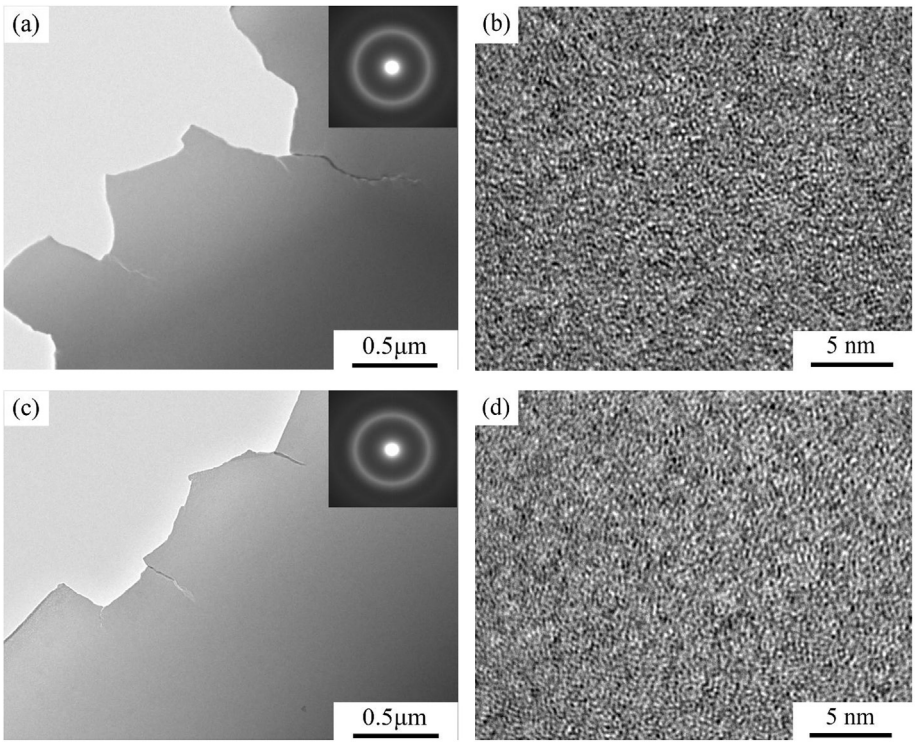

Fig. 2. TEM bright-field images, selected area electron diffraction (SAED) patterns and high-resolution transmission electron microcopy (HRTEM) images of $Zr_{55}Ti_3Hf_xCu_{32-x}Al_{10}$ ($x = 0$ and 3 at.%) alloys with the critical diameters: (a), (b) $x = 0$, Φ4mm, (c), (d) $x = 3$, Φ8mm.

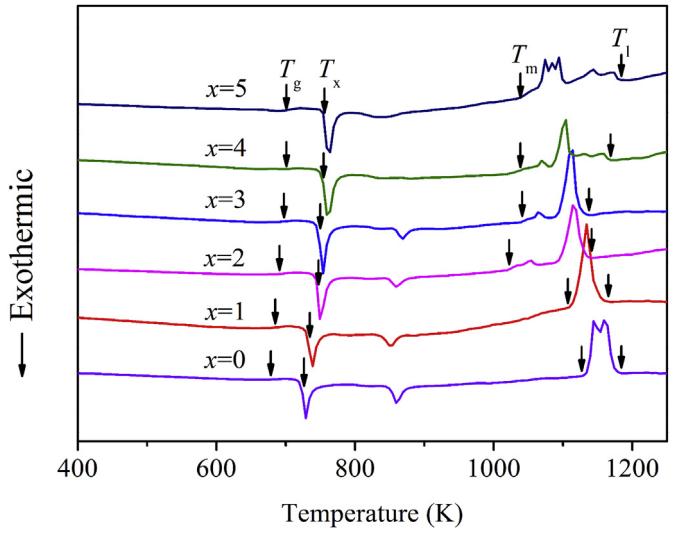

Fig. 3. DSC curves of $Zr_{55}Ti_3Hf_xCu_{32-x}Al_{10}$ ($x = 0$, 1, 2, 3, 4 and 5 at.%) with a heating rate of 20 K/min.

for the alloys with different Cu/Hf ratio, as shown in Table 2. The addition of Hf increased the complexity of alloy formulation, resulting in an increase in the mixing entropy (ΔS_{mix}) values in the Zr–Ti–Cu–Al BMGs system. In addition, the mixing enthalpy (ΔH_{mix}) have a relatively high value [33,38], which changes slightly. Increasing the ΔS_{mix} as well as the complexity of alloy composition promoted the enhancement of GFA of BMGs [14,15]. It is believed that the presence of multiple components with the addition of Hf assisted in stabilizing the liquid structure against crystalline phases during solidification. The addition of Hf with large atomic sizes will increase the distribution of atomic size [30]. With increase in δ and $\Delta\chi$ values, the formation of a dense packing structure is favored and the long-range rearrangement of these elements is restrained, leading to an increase in GFA [31,34]. However, the GFA is not always increased with the enhancement of $\Delta\chi$ and δ values. The formation of compound was promoted own to excessively large $\Delta\chi$. Excessive δ values do not ensure a high dense packing structure in amorphous alloys. In a word, there was an optimum δ in a given BMGs system in term of GFA [31]. With the decrease of δ values, high GFA of BMGs was also obtained. $\Delta\chi$ values almost does not change and the effect on the GFA of amorphous was not reflected in present BMGs system. The VEC value also has weak impact on the

Table 1
Thermal parameters of $Zr_{55}Ti_3Hf_xCu_{32-x}Al_{10}$ ($x = 0$, 1, 2, 3, 4 and 5 at.%).

Alloys	T_g(K)	T_x(K)	T_m(K)	T_l(K)	ΔT(K)	T_{rg}	γ
0	668	723	1129	1188	55	0.562	0.389
1	670	728	1024	1179	58	0.568	0.394
2	676	746	1040	1127	70	0.599	0.413
3	677	746	1020	1124	69	0.603	0.414
4	694	751	1021	1163	57	0.597	0.404
5	697	756	1039	1180	59	0.591	0.403

Table 2
Calculated parameters ΔH_{mix}, δ, $\Delta\chi$, ΔS_{mix} and VEC for $Zr_{55}Ti_3Hf_xCu_{32-x}Al_{10}$ ($x = 0$, 1, 2, 3, 4 and 5 at.%).

Alloys	δ	$\Delta\chi$	ΔH_{mix}(kJ·mol^{-1})	ΔS_{mix}(J·K^{-1}·mol^{-1})	VEC
0	9.95	0.26	−26.70	8.55	6.14
1	9.86	0.25	−27.05	8.92	6.07
2	9.76	0.25	−26.38	9.17	6.00
3	9.66	0.25	−26.20	9.38	5.93
4	9.56	0.25	−25.91	9.56	5.86
5	9.45	0.25	−25.80	9.71	5.79

formation of amorphous, which plays a crucial role in determining the type of solid solution in HEAs [28,32]. Additionally, main components that have large negative heat of mixing values were also beneficial for the formation of BMGs [35,37]. In Zr-Hf-Ti-Cu-Al amorphous alloy system, the large negative heat of mixing values for Hf–Cu and Hf–Al were −39 kJ/mol and −17 kJ/mol, respectively. That suggested that Hf with Cu and Al atoms formed preferable atomic pairs in supercooled liquid region. The interactions among the compositions could be improved, thereby promoting the chemical short-range order. This was beneficial in enhancing the local atomic packing efficiency and restraining long range diffusion of atoms. Consequently, the liquid phase became more stable, leading to the enhancement of GFA. However, further addition of Hf content had a negative effect on the improvement of GFA. Because of the positive heat of mixing of 0 kJ/mol for Hf–Zr, and 0 kJ/mol for Hf–Ti in this system, the strong atomic bonding of amorphous was deteriorated. The local atomic packing density was weakened [36] and finally resulted in the degradation of GFA.

Several parameters like T_{rg} and γ values are generally taken as indicators of GFA of BMGs [4,26]. Larger T_{rg} and γ indicated that the formation of amorphous alloy from the undercooled liquid was more easily and higher GFA. T_{rg} and γ values of alloys attained the maximum values of 0.603 and 0.414 for $x = 3$. The optimum GFA also occurred at the corresponding composition of $Zr_{55}Ti_3Hf_3Cu_{29}Al_{10}$. According to the above analysis, it can be concluded that the enhancement of GFA of the amorphous alloy was obtained by adding properly amount of Hf in present BMGs system.

3.3. Mechanical properties of BMGs

Fig. 4 shows the compressive stress–strain curves of $Zr_{55}Ti_3Hf_xCu_{32-x}Al_{10}$ ($x = 0$, 1, 2, 3, 4 and 5 at.%) alloys rod with a diameter of 3 mm under uniaxial compression at room temperature. Table 3 also summarizes the compressive test results, including fracture strength (σ_f), elastic strain (ε_e), the compressive yield strength (σ_y), plastic strain (ε_p), and Young's modulus (E). The original $Zr_{55}Ti_3Cu_{32}Al_{10}$ alloy had a compressive fracture strength of about 1695 ± 24 MPa without any plastic deformation stage. A large elastic deformation of approximately 2% was exhibited and begin to yield. After yielding, a distinct plastic flow accompanied by serration was observed for BMGs. The largest plastic strain of 2.60 ± 0.10% was obtained with 3 at. % Hf. Although the magnitude of strength and strain enhancement were different, all investigated

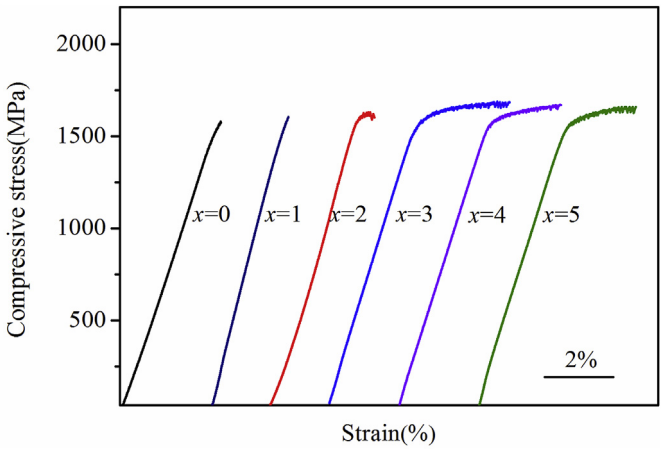

Fig. 4. The compressive stress–strain curves of $Zr_{55}Ti_3Hf_xCu_{32-x}Al_{10}$ ($x = 0$, 1, 2, 3, 4 and 5 at.%) alloys under uniaxial compression with a diameter of 3 mm at room temperature.

Table 3
Compressive mechanical properties of $Zr_{55}Ti_3Hf_xCu_{32-x}Al_{10}$ ($x = 0$, 1, 2, 3, 4 and 5 at.%) alloy rods with a diameter of 3 mm.

Alloy	σ_y (MPa)	σ_f (MPa)	ε_e (%)	ε_p (%)	E (GPa)
0	–	1695 ± 24	2.00 ± 0.03	0	85
1	–	1716 ± 11	2.10 ± 0.06	0	82
2	1745 ± 17	1771 ± 27	2.35 ± 0.04	0.25 ± 0.09	76
3	1800 ± 21	1824 ± 35	2.40 ± 0.10	2.60 ± 0.10	74
4	1771 ± 28	1793 ± 23	2.44 ± 0.11	1.64 ± 0.12	73
5	1765 ± 25	1780 ± 32	2.45 ± 0.09	1.63 ± 0.07	74

BMGs showed improvements when compared to the original amorphous composition. The Hf-bearing BMGs had Young's moduli (E) in the range of 74–85 GPa, which were obtained by calculating the linear part of the compressive stress-strain curves. The obtained E was lower than that of Ti–6Al–4V alloy ($E = 101$–125 GPa) and stainless steel (316LSS, $E = 193$–210 GPa), but close to human bones ($E = 20$–30 GPa) [5,40]. It is known that the mismatch of Young's modulus between implants and bone could cause bone resorption. Low Young's moduli are beneficial to alleviate the stress shielding effect. So preparation of BMGs in present study are beneficial for medical devices, implants and prosthesis applications. It can be seen that $Zr_{55}Ti_3Hf_3Cu_{29}Al_{10}$ alloy with a lower E not only exhibits high σ_y of 1800 ± 21 MPa but also shows the largest ε_p of 2.60 ± 0.1%. The result demonstrates that appropriate Hf addition can significantly enhance mechanical properties in present BMGs system.

The fracture and lateral surface morphology images of $Zr_{55}Ti_3Hf_xCu_{32-x}Al_{10}$ ($x = 0$, 1, 3 and 5 at. %) BMGs after final fracture are shown in Figs. 5 and 6. The fracture surface angle was found to be at 42° to the direction of the outside force loaded. From the fracture surface of the samples, we found formation of the typical vein patterns of the BMGs, which originated from shear deformation of the amorphous alloy. The distribution of the vein pattern and shear bands affect the plasticity of the BMGs. Generally, the density of vein-like patterns on fracture surface and the number of shear bands in lateral surface determined the plasticity of amorphous alloy. As can be seen from Fig. 5 (a)–(b), the morphology of mixed was composed of vein-like patterns and relatively smooth areas on the fracture surface of $Zr_{55}Ti_3Cu_{32}Al_{10}$ and $Zr_{55}Ti_3Hf_1Cu_{31}Al_{10}$ BMGs. Different from the mixed morphology, the observation of jagged vein-like patterns were obtained from the fracture surfaces of $Zr_{55}Ti_3Hf_3Cu_{29}Al_{10}$ samples. The vein patterns not only became more regular and well-developed, but the density of vein patterns also increased as compared to the other as-cast alloys. It is well known that the toughness of the samples may be estimated from the average scale of the vein patterns. The toughness K_C of BMGs can be estimated by using $r_p=(1/6\pi)(K_C/\sigma_y)^2$ [42,43], where r_p is the average dimensions of the vein patterns and σ_y the yield strength. The value of r_p and σ_y are about 31 μm and 1.77 GPa for $Zr_{55}Ti_3Hf_5Cu_{27}Al_{10}$ alloy. The K_C is calculated to be 44.13 MPa $m^{1/2}$, which is higher than other composition alloy in present BMGs.

Observation of different shear band morphologies in the SEM images were shown in Fig. 6. There was an obvious difference in the morphology and density of shear bands for the BMGs samples. Increasing Hf content resulted in a great deal of widely distributed shear bands on the lateral surface of $Zr_{55}Ti_3Hf_3Cu_{29}Al_{10}$ samples. The fluctuation of stress-strain curve after yield resulted in producing many single shear bands. It is noted that a great deal of shear bands was distributed in different direction on the samples surface, as shown in Fig. 6. Primary shear bands were approximately parallel to the direction of single shear plane. Most of shear bands deviated from the original direction and bifurcated. As the applied stress was increased, the high density of shear bands

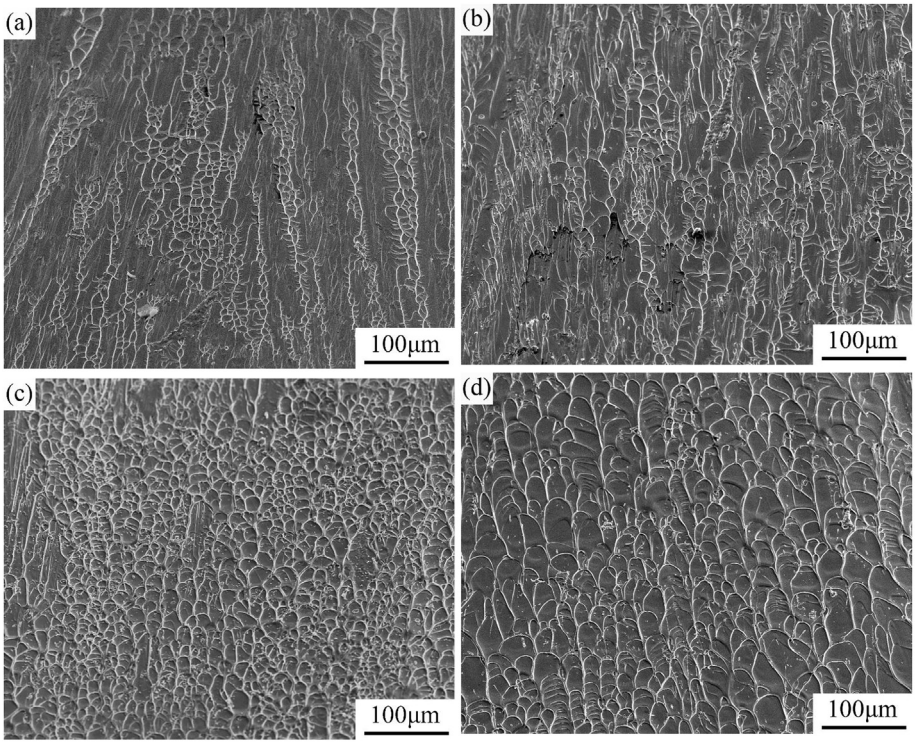

Fig. 5. SEM images of fracture morphologies for the $Zr_{55}Ti_3Hf_xCu_{32-x}Al_{10}$ ($x = 0$, 1, 3, 5 at.%) BMGs sample: (a) $x = 0$, (b) $x = 1$, (c) $x = 3$, (d) $x = 5$.

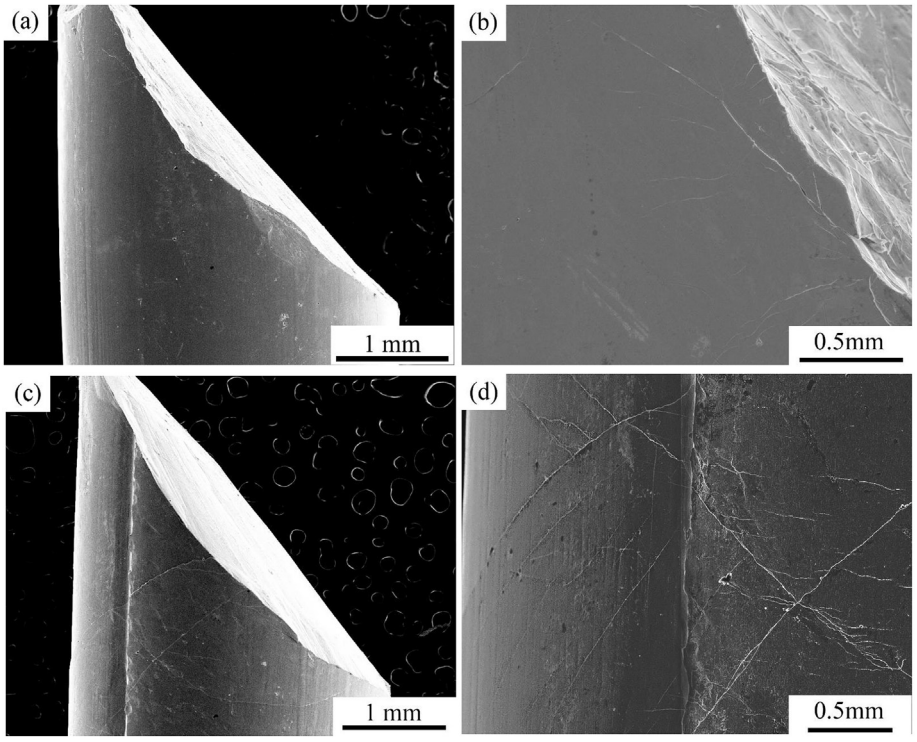

Fig. 6. SEM images of lateral surfaces of $Zr_{55}Ti_3Hf_xCu_{32-x}Al_{10}$ ($x = 0$, 3 at.%) alloys with the diameter of 3 mm after compressive tests. (a) $Zr_{55}Ti_3Cu_{32}Al_{10}$ with a low magnification; (b) the local area of lateral surface in (a); (c) $Zr_{55}Ti_3Hf_3Cu_{29}Al_{10}$ with a low magnification; (d) the local area of lateral surface in (c).

interacted with each other, leading to the intersection and branching of shear bands. In addition, the propagation of the shear bands were suppressed along one single shear direction due to the formation of multiple shear bands [41,44]. Highlighted shear steps and ledges related to the shear band movement were also observed. The density of shear bands have a significant benefit on the degree of plastic deformation of BMGs [35,39]. Small amounts of branching of shear bands also enhanced the plasticity of BMGs. It

can be seen that production of a great deal of shear bands from the outside surface of the BMGs specimens, leading to the generation of large plasticity of amorphous alloy.

According to recent reports, the enhancement of plasticity of amorphous alloys was obtained by adding appropriate alloy elements. Owing to the addition of elements with a positive mixed heat, the atomic bonding structure of the amorphous alloy was changed [45,46], resulting in the local region chemical inhomogeneity. In addition, the distribution of local free volume also changed or fluctuate in the single amorphous matrix [47]. In Zr-Hf-Ti-Cu-Al system, both Ti—Hf, Zr—Hf atomic pairs had a positive heat of mixing of 0 kJ/mol, which resulted in local structural inhomogeneity due to repulsive interactions between atoms. The local structural inhomogeneity in the BMGs can be used as the initiation sites for shear bands. In addition, this causes the production of a number of shear bands, resulting in large plastic deformation in BMGs [48]. The concept of the free volume model can helps us to explain the plasticity of amorphous alloys. It assumes that the addition of elements causes composition fluctuation of BMGs, resulting in higher free volumes stored in the amorphous alloy matrix [49]. According to Spaepen and Argon [50], the fluctuation of free volume is beneficial to the operation and formation of shear transformation zones (STZs) [45]. Liu et al. proposed a core-shell structure based on the free volume model [51]. The core is the density packed region with less free volume, and the surrounding with higher free volume acts as the shell. Upon plastic deformation, the shell as the initiation region favorable facilitates the production of shear bands, while the core usually inhibits the propagation of shear bands. The nucleation, multiplication branching and deflection of shear bands are activated under outside loading, leading to the improvement of plasticity of the BMGs.

In present study, owing to partial substitution of Cu by Hf causes structural heterogeneity, which results in the production of a large amount of free volume in amorphous matrix. Therefore, the activation of STZs and the formation and propagation of shear bands enhanced the room temperature plasticity of BMGs [52]. In summary, the Zr—Ti-Hf-Cu-Al BMGs showed superior plastic deformation than the Hf-free BMG under compressive loading.

3.4. Corrosion behavior

To investigate the influence of Hf content on the corrosion behavior of $Zr_{55}Ti_3Hf_xCu_{32-x}Al_{10}$ ($x = 0$, 1, 3 and 5 at. %) BMGs, electrochemistry tests were conducted in various solutions at room temperature under open air conditions, including 0.6 mol/L NaCl, 1 mol/L HCl, and 1 mol/L H_2SO_4 solutions. Fig. 7 (a)-(c) shows the experimental results of the novel developed Zr-based BMGs in different solutions for comparison. Table 4 is the relevant electrochemical parameters of amorphous alloy, including the corrosion potential (E_{corr}), corrosion current densities (I_{corr}) and pitting potential (E_{pit}). Fig. 7 (a) shows similar polarization behaviors of BMGs samples in 0.6 mol/L NaCl solution. As the decrease current density, cathodic polarization initially occurred, and after reaching a minimum value, the anodic polarization gradually increased in the current density. As the Hf content increases from 0 to 5 at.%, a rapid enhancement of the corrosion current densities was observed, and the E_{pit} increased from about -242 ± 36 mV to -18 ± 18 mV, which indicated the occurrence of pitting corrosion. As Hf content reached 5 at.%, E_{corr} increased to -295 ± 16 mV from -403 ± 27 mV and I_{corr}, which was obtained by the Tafel slope method, dropped to about $3.7 \pm 0.2 \times 10^{-8}$ A/cm^2. As shown in Fig. 7 (b) in 1 mol/L HCl solution, the BMGs exhibited a polarization behavior that was similar to the 0.6 mol/L NaCl solution. However, all the alloys showed rapid active dissolution at negative potentials without any pitting. E_{corr} also increased from -468 ± 22 mV to -298 ± 34 mV as the Hf content increased from 0 to 5 at. %. I_{corr} decreased from $4.2 \pm 0.4 \times 10^{-7}$ A/cm^2 to $8.0 \pm 0.2 \times 10^{-8}$ A/cm^2 for Zr-based BMGs. Fig. 7 (c) shows the polarization curves of as-cast alloys in 1 mol/L H_2SO_4 solution, where all alloys showed excellent passivation behavior. This result was different from the corrosion behavior in HCl and NaCl solutions. As the anodic polarization potential increase, the polarization curve gradually enters a stable passive region after the beginning of the anodic polarization. The transition from activation to passivation was not observed. As shown in Fig. 7 (c), as the applied potential increase, the I_{corr} slowly changed on the anodic polarization curves, indicating that a stable passive film was produced on the specimen surface in H_2SO_4 solution. Furthermore, E_{corr} slightly increased from -207 ± 15 mV to -156 ± 22 mV, and I_{corr} decreased from $2.5 \pm 0.3 \times 10^{-8}$ A/cm^2 to $1.6 \pm 0.1 \times 10^{-8}$ A/cm^2.

By analyzing the polarization curves, the corrosion resistance of amorphous alloys obviously were affected by the content of Hf addition in various solutions. Especially in NaCl solution, the E_{pit} was further enhanced due to the addition of Hf to the Zr-based BMGs, which increases from -242 ± 36 mV to -18 ± 18 mV. E_{pit} as an indicator of the pitting corrosion resistance for amorphous alloy, and a higher E_{pit} indicate better pitting corrosion resistance for materials. However, in HCl solution, all the specimens showed a rapid anodic active dissolution, indicating the absence of any pitting-corrosion event. Moreover, I_{corr} also significantly decreased by an order of magnitude with increasing in the content of Hf from $x = 0$ to $x = 5$, suggesting that the enhancement of the corrosion resistance was also obtained owing to the Hf addition. The corrosion behavior exhibited significant difference in 1 mol/L H_2SO_4 solution, all BMGs show a distinctly passive behavior compared to in NaCl and HCl solutions, indicating the formation of a protective passive film on the surface after polarization. The lowest I_{corr} was obtained ($1.6 \pm 0.1 \times 10^{-8}$ A/cm^2) for the samples with the Hf content of $x = 5$ after the polarization. In general, smaller I_{corr} and higher E_{corr} indicated excellent chemical stability and lower corrosion rates in materials. Therefore, the Hf-bearing BMGs showed better corrosion resistance in H_2SO_4 solution than HCl and NaCl solutions.

Furthermore, numerous studies have revealed that Hf, Al, Nb and Ti are valve metal elements, which evidently improve the corrosion resistance owing to a passive film on the surface of Zr-based BMGs in various solutions [53,54]. In general, the corrosion resistance of amorphous alloys with high content Cu is inferior compared with the Cu-free BMGs, since Cu has a strong affinity with chloride ion to form metal chlorides which promote the nucleation of pits, and eventually leads to the breakdown of the surface passive film. In this work, the addition of Hf may promote the passive film formation of the surface between the alloys and electrolytes solutions. Thus, this prevents their direct contact and further impedes the reaction, which then enhanced the corrosion resistance of the BMGs [55,56]. Therefore, the electrochemical measurements further demonstrate that the substitution of Cu with Hf can observably improve the corrosion resistance of $Zr_{55}Ti_3Hf_xCu_{32-x}Al_{10}$ ($x = 0$, 1, 3 and 5 at. %) BMGs in different solutions.

4. Conclusions

In this work, the influence of the substitution of Cu with Hf on GFA, mechanical properties and corrosion resistance of $Zr_{55}Ti_3Hf_xCu_{32-x}Al_{10}$ ($x = 0$, 1, 2, 3, 4 and 5 at.%) alloys are summarized as follows:

(1) Partial substitution Hf significantly promoted the GFA and the thermal stability. Zr55Ti3Hf3Cu29Al10 alloy with a maximum diameter of 8 mm was successively fabricated. Trg

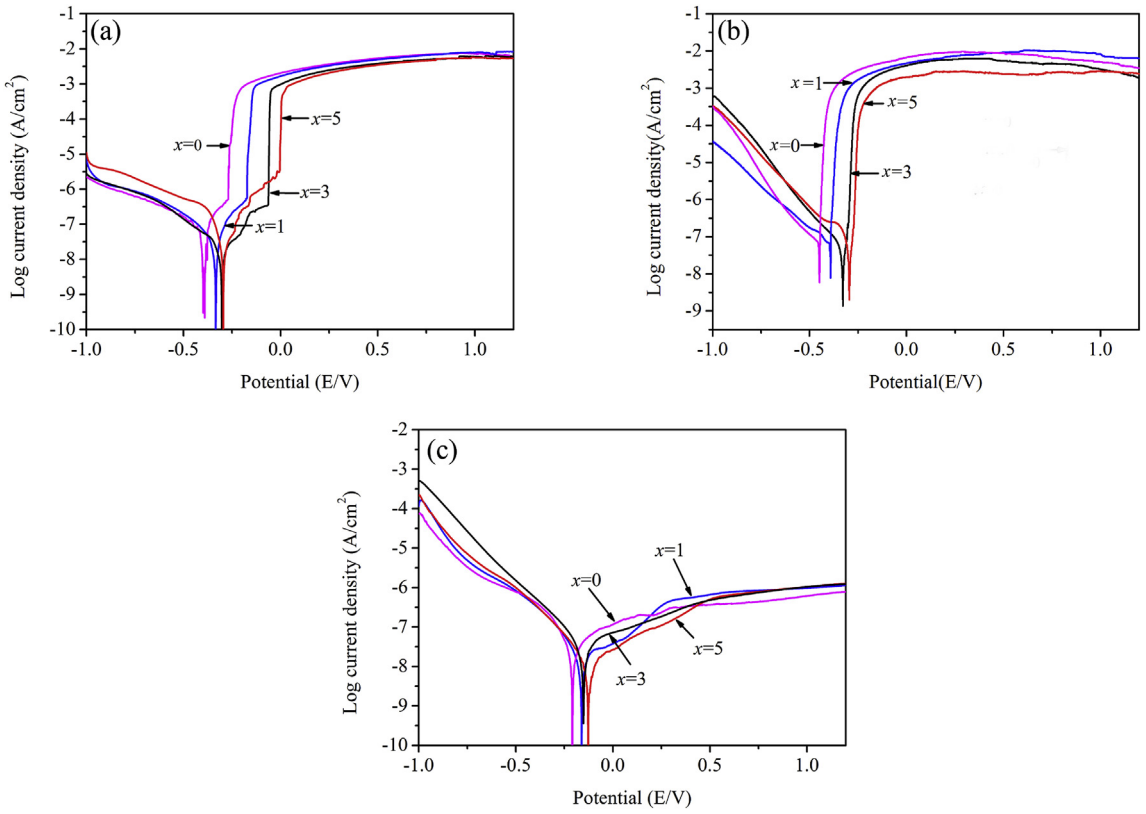

Fig. 7. Polarization curves of the $Zr_{55}Ti_3Hf_xCu_{32-x}Al_{10}$ ($x = 0$, 1, 2, 3, 4 and 5 at.%) BMGs in different solutions at room temperature: (a) 0.6 mol/L NaCl, (b) 1 mol/L HCl, (c) 1 mol/L H_2SO_4.

Table 4
Electrochemical parameters of $Zr_{55}Ti_3Hf_xCu_{32-x}Al_{10}$ ($x = 0$, 1, 3 and 5 at.%) alloys after polarization in different solutions.

Solutions	Compositions	I_{corr} (A/cm^2)	E_{corr} (mV)	E_{pit} (mV)
NaCl	$x = 0$	$4.2 \pm 0.4 \times 10^{-8}$	-403 ± 27	-242 ± 36
	$x = 1$	$4.0 \pm 0.2 \times 10^{-8}$	-334 ± 14	-201 ± 41
	$x = 3$	$3.8 \pm 0.3 \times 10^{-8}$	-296 ± 17	-43 ± 29
	$x = 5$	$3.7 \pm 0.2 \times 10^{-8}$	-295 ± 16	-18 ± 18
HCl	$x = 0$	$4.2 \pm 0.4 \times 10^{-7}$	-468 ± 22	–
	$x = 1$	$2.1 \pm 0.3 \times 10^{-7}$	-399 ± 15	–
	$x = 3$	$1.2 \pm 0.2 \times 10^{-7}$	-325 ± 28	–
	$x = 5$	$8.0 \pm 0.2 \times 10^{-8}$	-298 ± 34	–
H_2SO_4	$x = 0$	$2.5 \pm 0.3 \times 10^{-8}$	-207 ± 15	–
	$x = 1$	$2.4 \pm 0.2 \times 10^{-8}$	-202 ± 12	–
	$x = 3$	$1.8 \pm 0.3 \times 10^{-8}$	-165 ± 21	–
	$x = 5$	$1.6 \pm 0.1 \times 10^{-8}$	-156 ± 22	–

and γ values of alloys attained the maximum values of 0.603 and 0.414 for x = 3. The width of supercooled liquid region was increased by 15 K for the prepared alloys.

(2) The mechanical properties were improved after adding an appropriate amount of Hf. Zr55Ti3Hf3Cu29Al10 possessed the largest plastic strain of $2.60 \pm 0.10\%$ and ultimate compressive strength up to 1824 ± 35 MPa.

(3) Different corrosion behaviors were observed after polarization in various solutions. Obvious pitting corrosion occurred in chloride-ion containing solutions, whereas a stable passivation behavior was observed in H2SO4 solution. The lowest corrosion current density was $1.6 \pm 0.1 \times$ 10-8 A/cm2 after polarization in H2SO4 solution. All results demonstrate that the substitution of Cu with Hf can effectively enhance the corrosion resistance of the BMGs.

Acknowledgement

The research was supported by NSFC (51671166/51827801/51434008).

References

[1] W.H. Wang, C. Dong, C.H. Shek, Bulk metallic glasses, Mater. Sci. Eng. R. 44 (2004) 45–89.
[2] C.J. Byrne, M. Eldrup, Bulk metallic glasses, Mater. Sci. Eng. R. 321 (2008) 502–503.
[3] A. Takeuchi, A. Inoue, Classification of bulk metallic glasses by atomic size difference, heat of mixing and period of constituent elements and its application to characterization of the main alloying element, Mater. Trans. 46 (2005) 2817–2829.
[4] A. Inoue, Stabilization of metallic supercooled liquid and bulk amorphous alloys, Acta Mater. 48 (2000) 279–306.
[5] Q. Chen, G.A. Thouas, Metallic implant biomaterials, Mater. Sci. Eng. R. 87 (2015) 1–57.
[6] R. Busch, S. Schneider, A. Peker, W.L. Johnson, Decomposition and primary crystallization in undercooled $Zr_{41.2}Ti_{13.8}Cu_{12.5}Ni_{10.0}Be_{22.5}$ melts, Appl. Phys. Lett. 67 (1995) 1544–1546.
[7] A. Inoue, W. Zhang, T. Zhang, K. Kurosaka, High-strength Cu-based bulk glassy alloys in Cu–Zr–Ti and Cu–Hf–Ti ternary systems, Acta Mater. 49 (2001) 2645–2652.
[8] H. Ma, L.L. Shi, J. Xu, Y. Li, E. Ma, Discovering inch-diameter metallic glasses in three-dimensional composition space, Appl. Phys. Lett. 87 (2005) 181915.
[9] Z.P. Lu, C.T. Liu, Role of minor alloying additions in formation of bulk metallic glasses: a Review, J. Mater. Sci. 39 (2004) 3965–3974.
[10] X.H. Lin, W.L. Johnson, Formation of Ti–Zr–Cu–Ni bulk metallic glasses, Appl. Phys. Lett. 78 (1995) 6514–6519.
[11] Y. Li, W. Zhang, F. Qin, A. Makino, Mechanical properties and corrosion resistance of a new $Zr_{56}Ni_{20}Al_{15}Nb_4Cu_5$ bulk metallic glass with a diameter up to 25mm, J. Alloy. Comp. 615 (2014) S71–S74.
[12] W.L. Johnson, Bulk amorphous metal—an emerging engineering material, J. Occup. Med. 54 (2002) 40–43.
[13] J.C. Wataha, P.E. Lockwood, A. Schedle, Effect of silver, copper, mercury, and nickel ions on cellular proliferation during extended, low-dose exposures, J. Biomed. Mater. Res. 52 (2000) 360–364.

[14] W.H. Wang, Z. Bian, P. Wen, Y. Zhang, M.X. Pan, D.Q. Zhao, Role of addition in formation and properties of Zr-based bulk metallic glasses, Intermetallics 10 (2002) 1249–1257.
[15] W.H. Wang, Roles of minor additions in formation and properties of bulk metallic glasses, Prog. Mater. Sci. 52 (4) (2007) 540–596.
[16] Y.J. Yang, B.Y. Cheng, J.W. Lv, B. Li, M.Z. Ma, X.Y. Zhang, G. Li, R.P. Liu, Effect of Ag substitution for Ti on glass-forming ability, thermal stability and mechanical properties of Zr-based bulk metallic glasses, Mater. Sci. Eng. A 746 (2019) 229–238.
[17] J.C. Qiao, Y. Yao, J.M. Pelletier, L.M. Keer, Understanding of micro-alloying on plasticity in $Cu_{46}Zr_{47-x}Al_7Dy_x$ ($0 \le x \le 8$) bulk metallic glasses under compression: based on mechanical relaxations and theoretical analysis, Int. J. Plast. 82 (2016) 62–75.
[18] Q.K. Jiang, X.D. Wang, X.P. Nie, G.Q. Zhang, H. Ma, H.J. Fecht, J. Bendnarcik, H. Franz, Y.G. Liu, Q.P. Cao, Zr–(Cu,Ag)–Al bulk metallic glasses, Acta Mater. 56 (2008) 1785–1796.
[19] Z. Wei, Q. Zhang, A. Inoue, Fabrication of Cu–Zr–Ag–Al glassy alloy samples with a diameter of 20 mm by water quenching, J. Mater. Res. 23 (2008) 1452–1456.
[20] Q. Zhang, W. Zhang, A. Inoue, Fabrication of new $Cu_{34}Pd_2Zr_{48}Ag_8Al_8$ bulk glassy alloy with a diameter of 30 mm, Mater. Trans. 48 (2007) 3031–3033.
[21] N. Hua, L. Huang, J. Wang, Y. Cao, W. He, S. Pang, T. Zhang, Corrosion behavior and in vitro biocompatibility of Zr-Al-Co-Ag bulk metallic glasses: an experimental case study, J. Non-Cryst. Solids 358 (2012) 1599–1604.
[22] H.F. Li, Y.F. Zheng, F. Xu, J.Z. Jiang, In vitro investigation of novel Ni free Zr-based bulk metallic glasses as potential biomaterials, Mater. Lett. 75 (2012) 74–76.
[23] L. Liu, C.L. Qiu, Q. Chen, Corrosion behavior of Zr-based bulk metallic glasses in different artificial body fluids, J. Alloy. Comp. 425 (2006) 268–273.
[24] D. Qiao, A. Peker, Enhanced glass forming ability in Zr-based bulk metallic glasses with Hf Addition, Intermetallics 24 (2012) 115–119.
[25] C.L. Qin, W. Zhang, K. Asami, H. Kimura, X.M. Wang, A. Inoue, A novel Cu-based BMG composite with high corrosion resistance and excellent mechanical properties, Acta Mater. 54 (2006) 3713–3719.
[26] Z.P. Lu, C.T. Liu, A new glass-forming ability criterion for bulk metallic glasses, Acta Mater. 50 (2002) 3501–3512.
[27] W.H. Wang, Q. Wei, S. Friedrich, Microstructure, decomposition, and crystallization in $Zr_{41}Ti_{14}Cu_{12.5}Ni_{10}Be_{22.5}$ bulk metallic glass, Phys.Rev. 57 (1998) 8211–8217.
[28] S. Guo, C.T. Liu, Phase stability in high entropy alloys:Formation of solid-solution phase or amorphous phase, Prog. Nat. Sci. Mater. Int. 21 (6) (2011) 433–446.
[29] A. Takeuchi, A. Inoue, Classification of bulk metallic glasses by atomic size difference, heat of mixing and period of constituent elements and its application to characterization of the main alloying element, Mater. Trans. 46 (12) (2005) 2817–2829.
[30] H.X. Li, Z.C. Lu, S.L. Wang, et al., Fe-based bulk metallic glasses: glass formation, fabrication, properties and applications[, Prog. Mater. Sci. 103 (2019) 235–318.
[31] Z.P. Lu, C.T. Liu, Y.D. Dong, Effects of atomic bonding nature and size mismatch on thermal stability and glass-forming ability of bulk metallic glasses, J. Non-Cryst. Solids 341 (1–3) (2004) 0–100.
[32] S. Guo, C. Ng, J. Lu, et al., Effect of valence electron concentration on stability of fcc or bcc phase in high entropy alloys, J. Appl. Phys. 109 (10) (2011) 213.
[33] Y. Zhang, Y. Zhou, J. Lin, et al., Solid-solution phase formation rules for multi-component alloys, Adv. Eng. Mater. 10 (6) (2008) 534–538.
[34] S. Fang, Xueshan Xiao, Lei Xia, et al., Relationship between the widths of supercooled liquid regions and bond parameters of Mg-based bulk metallic glasses, J. Non-Cryst. Solids 321 (1) (2003) 120–125.
[35] Y. Li, W. Zhang, C. Dong, C. Qin, J. Qiang, A. Makino, A. Inoue, Enhancement of glass-forming ability and corrosion resistance of Zr-based Zr-Ni-Al bulk metallic glasses with minor addition of Nb, J. Appl. Phys. 110 (2011) 42.
[36] S. H W, L. W K, A. F M, B. J M, M. E, Atomic packing and short-to-medium-range order in metallic glasses, Nature 439 (2006) 419–425.
[37] David Turnbull, Under what conditions can a glass be formed? Contemp. Phys. 10 (1969) 473–488.
[38] Y. Zhang, Y. Zhou, J. Lin, et al., Solid-solution phase formation rules for multi-component alloys, Adv. Eng. Mater. 10 (6) (2008) 534–538.
[39] C.L. Qiu, M. Sun, Q. Chen, K.C. Chan, G. Pang, Improvements in the plasticity and biocompatibility of Zr–Cu–Ni–Al bulk metallic glass by the microalloying of Nb, Mater. Sci. Eng. A 449 (2007) 193–197.
[40] N. Hua, L. Huang, W. Chen, W. He, T. Zhang, Biocompatible Ni-free Zr-based bulk metallic glasses with high-Zr-content: compositional optimization for potential biomedical applications, Mater.Sci. Eng. C. Mater. Biol. Appl. 44 (2014) 400–410.
[41] R.D. Conner, Y. Li, W.D. Nix, W.L. Johnson, Shear band spacing under bending of Zr-based metallic glass plates, Acta Mater. 52 (2004) 2429–2434.
[42] J.J. Lewandowski, W.H. Wang, A.L. Greer, Intrinsic plasticity or brittleness of metallic glasses, Philos. Mag. Lett. 85 (2) (2005) 77–87.
[43] X.K. Xi, D.Q. Zhao, M.X. Pan, et al., Fracture of brittle metallic glasses: brittleness or plasticity, Phys. Rev. Lett. 94 (12) (2005) 125510.
[44] J.C. Qiao, Y.J. Wang, J.M. Pelletier, L.M. Keer, M.E. Fine, Y. Yao, Characteristics of stress relaxation kinetics of La60Ni15Al25 bulk metallic glass, Acta Mater. 98 (2015) 43–50.
[45] E.S. Park, D.H. Kim, T. Ohkubo, K. Hono, Enhancement of glass forming ability and plasticity by addition of Nb in Cu–Ti–Zr–Ni–Si bulk metallic glasses, J. Non-Cryst. Solids 351 (2005) 1232–1238.
[46] H. Yin, Y. Huang, D. Daisenberg, P. Xue, S. Jiang, W. Ru, S. Jiang, Y. Bao, X. Bian, X. Tong, H. Shen, J. Sun, Atomic structure evolution of high entropy metallic glass microwires at cryogenic temperature, Scr. Mater. 163 (2019) 29–33.
[47] J.C. Qiao, Q. Wang, J.M. Pelletier, H. Kato, R. Casalini, D. Crespo, E. Pineda, Y. Yao, Y. Yang, Structural heterogeneities and mechanical behavior of amorphous alloys, Prog. Mater. Sci. 104 (2019) 250–329.
[48] K.B. Kim, J. Das, F. Baier, M.B. Tang, W.H. Wang, J. Eckert, Heterogeneity of a $Cu_{47.5}Zr_{47.5}Al_5$ bulk metallic glass, Appl. Phys. Lett. 88 (2006) 407.
[49] J. Li, C.H. Ke, X. Tong, Y.F. Jia, S.W. Wu, Y.D. Jia, J. Yi, G. Wang, Impact of free volume on shear band multiplication and bending plasticity, Mater. Sci. Eng. A 747 (2019) 136–143.
[50] F. Spaepen, A microscopic mechanism for steady state inhomogeneous flow in metallic glasses, Acta Metall. 25 (1976) 407–415.
[51] X.J. Liu, G.L. Chen, X. Hui, T. Liu, Z.P. Lu, Ordered clusters and free volume in a Zr-Ni metallic glass, Appl. Phys. Lett. 93 (2008).
[52] L.Q. Xing, Y. Li, K.T. Ramesh, J. Li, T.C. Hufnagel, Enhanced plastic strain in Zr-based bulk amorphous alloys, Phys.Rev. 64 (2001) 607–611.
[53] Q.P. Cao, S. Peng, X.N. Zhao, X.D. Wang, D.X. Zhang, J.Z. Jiang, Effect of Nb substitution for Cu on glass formation and corrosion behavior of Zr-Cu-Ag-Al-Be bulk metallic glass, J. Alloy. Comp. 683 (2016) 22–31.
[54] L. Liu, C.L. Qiu, H. Zou, et al., The effect of the microalloying of Hf on the corrosion behavior of ZrCuNiAl bulk metallic glass, J. Alloy. Comp. 399 (2005) 0–148.
[55] C. Qin, W. Zhang, K. Asami, N. Ohtsu, A. Inoue, Glass formation, corrosion behavior and mechanical properties of bulk glassy Cu–Hf–Ti–Nb alloys, Acta Mater. 53 (2005) 3903–3911.
[56] K. Asami, C.L. Qin, T. Zhang, A. Inoue, Effect of additional elements on the corrosion behavior of a Cu–Zr–Ti bulk metallic glass, Mater. Sci. Eng. A 375–377 (2004) 235–239.